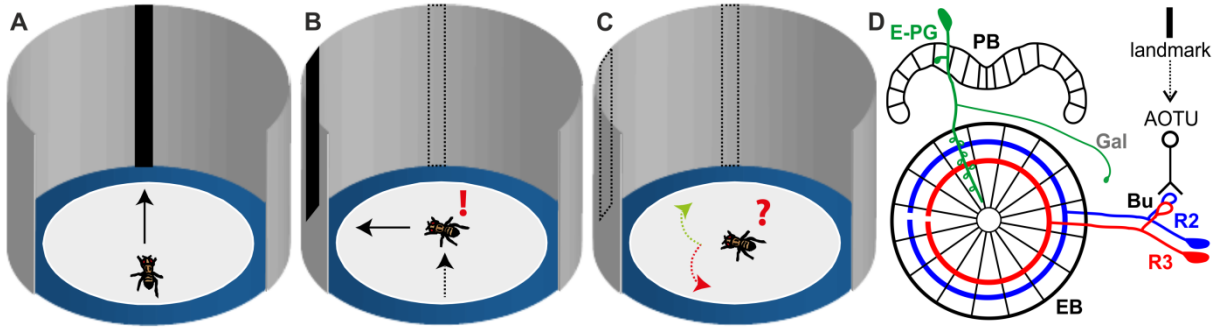

Figure S1. The detour paradigm for analysis of visual working memory, Related to Figure 1. (**A**) In the detour paradigm, a walking fly in a lit LED arena is heading towards a dark vertical stripe (landmark). (**B**) Just before crossing a virtual midline it is distracted by switching the stripe to + or -90°. This distractor stripe also disappears 1s after the fly has turned towards it; now no visual cues remain. (**C**) Turns of more than 45° in the direction of the initial landmark (green arrow) are counted as positive choices. Wild-type flies of both sexes recall the position of their initial target in ~80% of the trails and turn to resume their walk towards the original direction even when the landmark is still invisible. Note that the random choice level (dashed line in all box plots) is at 58% due to the so-called turn compensation. This value was determined by analyzing free walking flies in an arena without any cues. During random search a fly has a higher probability to perform a right turn after a previous left turn and *vice versa* [S1]. (**D**) Schematic drawing of the neuronal circuit involved in the visual working memory. At least four different types of ring neurons (~70 per hemisphere) project into the ellipsoid body (EB) where each of them has synaptic output sites in the 16 sectors (wedges) of the EB neuropil [S2, S3]. R neurons receive information about landmarks in their visual field through interneurons connecting the anterior optic tubercle (AOTU) with the dendritic field of R neurons in the bulb (Bu) [S4-S6]. Individual R2 neurons are activated by ipsilateral landmarks in their receptive flied and (together with R4 neurons; not depicted) hold a retinotopic representation of objects in the visual field of the fly [S7]. R3 neurons hold the memory trace for a vanished landmark [S8] and might respond with an off-signal when an object leaves the ipsilateral receptive field or are inhibited by contralateral objects [S4-S6]. Ring neurons synapse on “compass neurons” that innervate each wedge of the EB and receive information from the EB and project to one segment in the PB and the gal (E-PG neurons [S9, S10]). The neuronal activity in the E-PG neurons represents the relative position of the fly with respect to the objects. The signal moves from one compass neuron to the next one in a neighboring sector when the fly turns or the object is moving [S9].

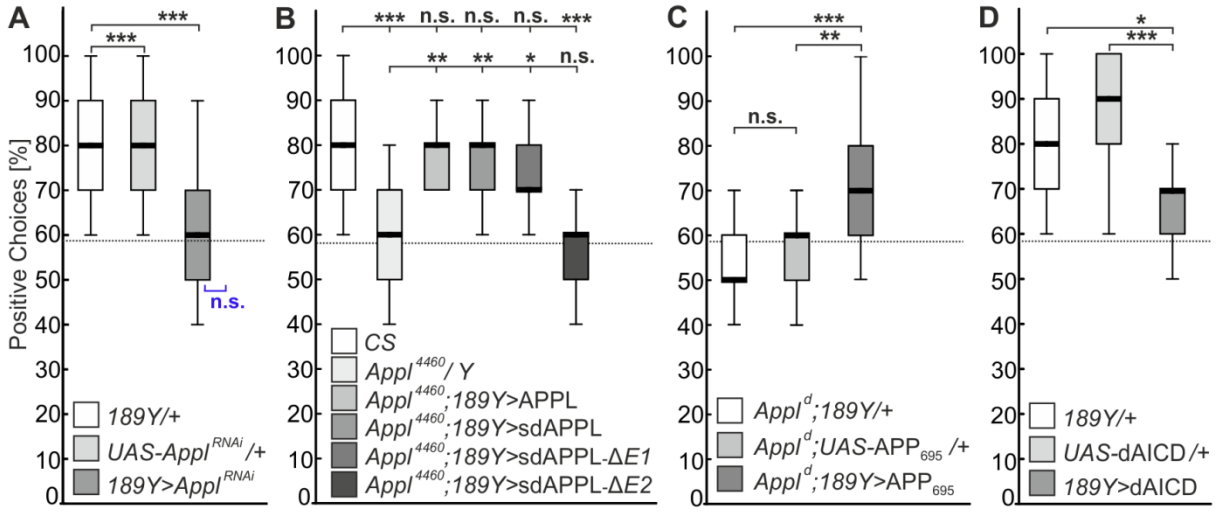

Figure S2. Requirement for APP_{695} or APPL in visual working memory, Related to Figure 2. (**A**) Inducing RNAi mediated knock downs of *Appl* in R3 neurons (*189Y*-GAL4) reduces the visual working memory to chance level. (**B**) Expression of full-length APPL and secretion-defective sdAPPL in R3 neurons can rescue the memory deficit of the hypomorphic $Appl^{4460}$ mutant to wild-type (CS) levels, whereas secretion defective sdAPPL-ΔE2 without the ecto-domain E2 does not rescue. In contrast deletion of ectodomain E1 (sdAPPL-ΔE1) does not affect the rescue ability. (**C**) Expression of human APP_{695} in R3 neurons can suppress the memory phenotype of the $Appl^{d}$ null-mutant to the same extent as full-length APPL (see Figure 2 in the main text). (**D**) Overexpression of *Drosophila* AICD in R3 neurons affects the working memory in comparison to controls. Boxes signify 25% / 75%-quartiles, thick lines medians and whiskers 10% / 90%-quantiles. The random choice level of 58% is shown by a dashed line. n = 25 males for all genotypes; age 3-5d; n.s., not significant; *, $p < 0.05$; **, $p < 0.001$; ***, $p < 0.001$. Shapiro-Wilk test for normal distribution; Kruskal-Wallis ANOVA, Bonferroni post-hoc. For statistical details see Data S2.

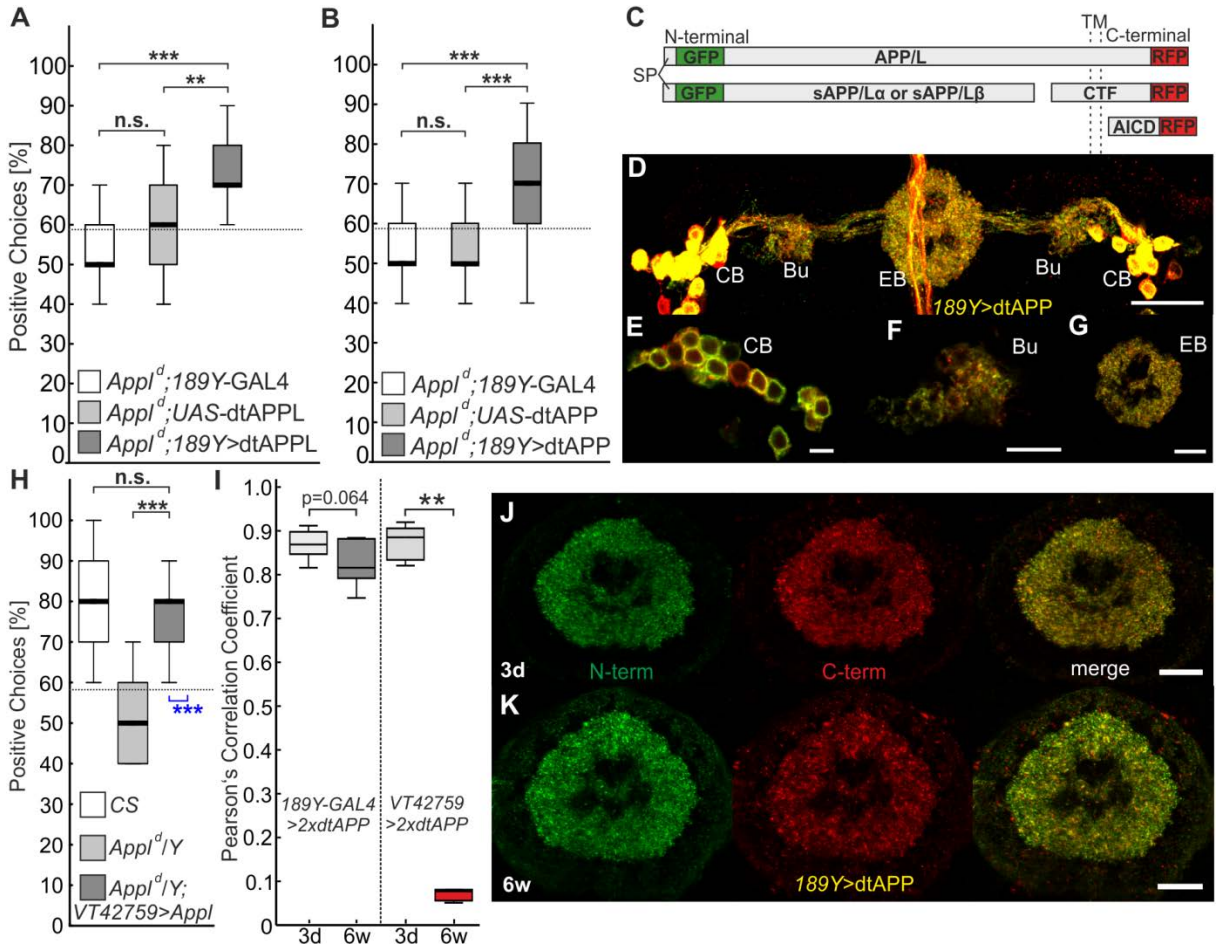

Figure S3. Evaluation of the double-tagged dtAPPL and dtAPP transgenes, Related to Figure 3. (**A**) Expression of the dtAPPL fusion protein in R3 neurons (*189Y*-GAL4) rescues the memory deficit of the *Appl*^{d} null-mutant to the same extent as wild-type APPL (see Figure 2A, 2B). (**B**) Expression of the human dtAPP fusion protein in R3 neurons also rescues the memory deficits of the *Appl*^{d} null-mutant to the same extent as wild-type APPL and dtAPPL. Boxes signify 25% / 75%-quartiles, thick lines medians and whiskers 10% / 90%-quantiles. The random choice level of 58% is shown by a dashed line. n = 25 males for all genotypes; age 3-5 days; n.s., not significant; *, $p < 0.05$; **, $p < 0.001$; ***, $p < 0.001$. Shapiro-Wilk test for normal distribution; Kruskal-Wallis ANOVA, Bonferroni post-hoc. For statistical details see Data S3. (**C**) Graphical illustration of the double tagged APP/L fusion proteins. Enhanced Green Fluorescent Protein (GFP) was cloned downstream of the APPL signal peptide (i.e. the first 27 amino acids) and Red Fluorescent Protein (RFP) was cloned in-frame with APPL or human APP_{695}, respectively. α-secretase or β-secretase cleavage results in a secreted, green fluorescent, N-terminal APP/L fragment. Subsequent γ-processing cleaves the red fluorescent C-terminal fragment (CTF), which results in the APP/L intracellular domain d/AICD that can translocate to the nucleus. (**D-G**) Distribution of full-length APP (yellow), secreted N-terminal APP (green), CTF (red), and AICD

(red) in the R3 neuron of the ellipsoid body. (**D**) Overview of R3 neurons projecting from the antero-lateral residing cell bodies (CB) to the dendritic arborization in the bulb (Bu) onto the axonal output sites in the ellipsoid body (EB; scale bar 25 µm; 45 µm z-projection). (**E**) In the cell bodies, most APP is processed but to different extent in individual cells. Note that in some cell bodies N-terminal fragments or CTFs are preferentially accumulated (scale bar 5 µm; 300 nm z-projection). (**F**) Full-length, cleaved N-terminal and C-terminal fragments can be found in the dendrites in the bulb neuropil (scale bar 10 µm; 300 nm z-projection). (**G**) Unprocessed dtAPP and cleaved fragments are localized at the axonal output sites in the EB (scale bar 10 µm; 300 nm z-projection). (**H**) The GAL4 driver line *VT42759* can rescue the memory deficit of the *Appl*^{d} mutant similar to *189Y*-GAL4 (significance to chance level in blue; n = 25 for all genotypes; Shapiro-Wilk test for normal distribution; Kruskal-Wallis ANOVA, Bonferroni post-hoc). (**I**) Co-localization analysis for N-terminal and C-terminal fragments produced from two copies of the dtAPP transgene expressed with the *189Y*-GAL4 or *VT42759*-GAL4 driver lines. Huygens software was used to calculate Pearson's correlation coefficient (value 1 would indicate absolute co-localization). n = 10 for 3 days and n = 7 for 6 week old *189Y*>dtAPP flies; n = 6 for 3 days and n = 5 for 6 week old *VT42759*>dtAPP flies. Shapiro-Wilk test for normal distribution; Mann-Whitney U-test for non-normal distributed data, unpaired t-test for normal distributed data. (**J-K**) 10 µm z-projection of *189Y*-GAL4 driven dtAPP expression in the ellipsoid body of 3 day (**J**) and 6 week (**K**) old flies (Scale bars 10 µm). Less yellow signal indicating less co-localization is seen; however, this is not statistically significant, as seen in (I).

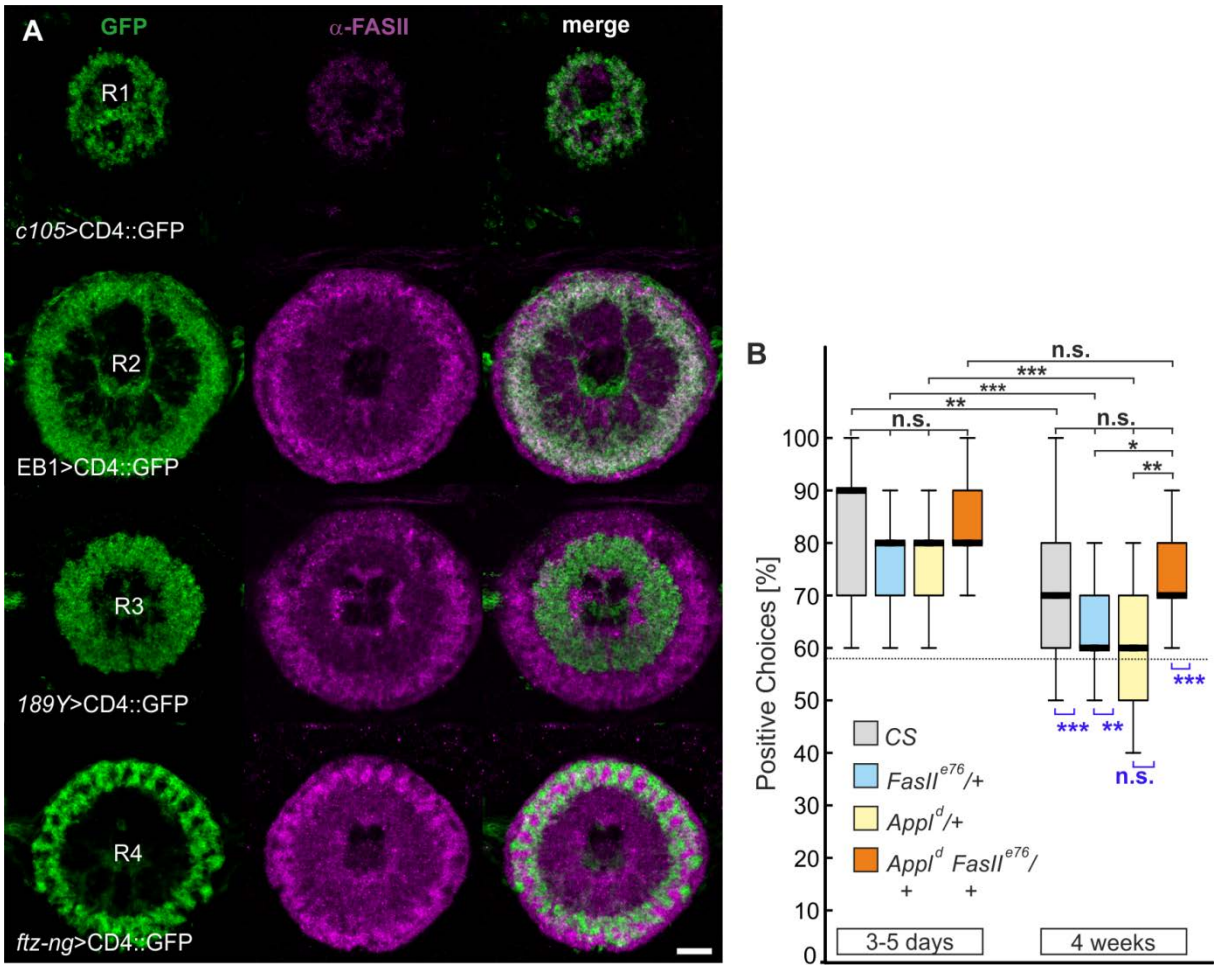

Figure S4. Expression analysis of the neuronal adhesion molecule FASII in the ellipsoid body and its role in age-related memory impairment (AMI), Related to Figure 4. (**A**) To analyze the localization of FASII in the axonal projections of different types of ring neurons [S2, S3, S8] in the ellipsoid body neuropil four cell-type specific GAL4 diver lines were used to express membrane bound tandem-GFP; note that FASII is strictly localized at the synaptic output sites of the ring neurons and barely visible in cell bodies, dendrites or axonal projections. Strong co-labeling of anti-FASII was found with the axonal projections of R2-neurons (UAS-CD4::tdGFP/II; EB1-GAL4/III) and R4-neurons (UAS-CD4::tdGFP/II; *ftz-ng*-GAL4/III) in the ellipsoid body. Less, but significant co-localization is seen within R3-neurons (*189Y*-GAL4/UAS-CD4::tdGFP) and limited expression of FASII is seen within axons of R1-neurons (*c105*-GAL4/X; UAS-CD4::tdGFP/II) scale bar 10 µm; 3 µm z-projection). (**B**) Neither heterozygous nor double heterozygous females for the hypomorphic *FasII*^{e76} allele or the *Appl*^{d} null-allele show a significant reduction in the visual working memory at the early age of 3-5 days. In contrast 4 week old wild-type flies show a reduced memory and heterozygous *Appl*^{d}/+ flies have lost their memory completely; i.e. they are not significantly different from chance level (indicated in blue). Additional heterozygosity for *FasII*^{e76} suppresses this AMI of *Appl*^{d}/+ flies. n = 25 for all geno-

types; n.s., not significant; *, $p < 0.05$; **, $p < 0.001$; ***, $p < 0.001$; Shapiro-Wilk test for normal distribution; Kruskal-Wallis ANOVA, Bonferroni post-hoc. For statistical details see Data S4.

Supplemental References:

S1. Strauss, R. and Pichler, J. (1998). Persistence of orientation toward a temporarily invisible landmark in *Drosophila melanogaster*. J. Comp. Physiol. A *182*, 411–423.

S2. Young, J.M., and Armstrong, J.D. (2010). Structure of the adult central complex in *Drosophila*: organization of distinct neuronal subsets. J. Comp. Neurol. *518*, 1500-1524.

S3. Martin-Pena, A., Acebes, A., Rodriguez, J.R., Chevalier, V., Casas-Tinto, S., Triphan, T., Strauss, R., and Ferrus, A. (2014). Cell types and coincident synapses in the ellipsoid *body of Drosophila. Eur. J. Neurosci. 39, 1586-1601.*

S4. Omoto, J.J., Keles, M.F., Nguyen, B.M., Bolanos, C., Lovick, J.K., Frye, M.A.,and Hartenstein, V. (2017). Visual input to the *Drosophila* central complex by developmentally and functionally distinct neuronal populations. Curr. Biol. *27*, 1098-1110.

S5. Sun, Y., Nern, A., Franconville, R., Dana, H., Schreiter, E.R., Looger, L.L., Svoboda, K., Kim, D.S., Hermundstad, A.M., and Jayaraman, V. (2017). Neural signatures of dynamic stimulus selection in *Drosophila*. Nat. Neurosci. *20*, 1104-1113.

S6. Shiozaki, H.M., and Kazama, H. (2017). Parallel encoding of recent visual experience and self-motion during navigation in *Drosophila*. Nat Neurosci *20*, 1395-1403.

S7. Seelig, J.D., and Jayaraman, V. (2013). Feature detection and orientation tuning in the *Drosophila* central complex. Nature *503*, 262-266.

S8. Kuntz, S., Poeck, B., and Strauss, R. (2017). Visual Working Memory Requires Permissive and Instructive NO/cGMP Signaling at Presynapses in the *Drosophila* Central Brain. Curr. Biol. *27*, 613-623.

S9. Seelig, J.D., and Jayaraman, V. (2015). Neural dynamics for landmark orientation and angular path integration. Nature *521*, 186-191.

S10. Xie, X., Tabuchi, M., Brown, M.P., Mitchell, S.P., Wu, M.N., and Kolodkin, A.L. (2017). The laminar organization of the *Drosophila* ellipsoid body is semaphorin-dependent and prevents the formation of ectopic synaptic connections. eLife *6*, e25328.